Final Project Report: Quantifying microbe-mineral interactions leading to remotely detectable induced polarization signals (Award #DE-SC0002280)

Principle Investigators:
Stephen Moysey, Clemson University (PI)
Delphine Dean, Clemson University (co-PI)
Dimitrios Ntarlagiannis, Rutgers University (co-PI)

Other Project Participants:
Na Hao, Clemson University (PhD Student)
Ruikai Chen, Clemson University (PhD Student)

1. Project Summary

The objective of this project was to investigate controls on induced polarization responses in porous media. The approach taken in the project was to compare electrical measurements made on mineral surfaces with atomic force microscopy (AFM) techniques to observations made at the column-scale using traditional spectral induced polarization measurements. In the project we evaluated a number of techniques for investigating the surface properties of materials, including the development of a new AFM measurement protocol that utilizes an external electric field to induce grain-scale polarizations that can be probed using a charged AFM tip.

The experiments we performed focused on idealized systems (i.e., glass beads and silica gel) where we could obtain the high degree of control needed to understand how changes in the pore environment, which are determined by biogeochemical controls in the subsurface, affect mechanisms contributing to complex electrical conductivity, i.e., conduction and polarization, responses. The studies we performed can be classified into those affecting the chemical versus physical properties of the grain surface and pore space.

Chemical alterations of the surface focused on evaluating how changes in pore fluid pH and ionic composition control surface conduction. These were performed as column flow through experiments where the pore fluid was exchanged in a column of silica gel. Given that silica gel has a high surface area due to internal grain porosity, high-quality data could be obtained where the chemical influences on the surface are clearly apparent and qualitatively consistent with theories of grain (i.e., Stern layer) polarization controlled by electrostatic surface sorption processes (i.e., triple layer theory). Quantitative fitting of the results by existing process-based polarization models (e.g., Leroy et al., 2008) has been less successful, however, due to what we have attributed to differences between existing models developed for spherical grains versus the actual geometry associated with the nano-pores in the silica gel, though other polarization processes, e.g., proton hopping along the surface (Skold et al., 2013), may also be a contributing factor. As an alternative model-independent approach to confirming the link between surface sorption and SIP we initiated a study that will continue (unfunded) beyond the completion of this project to independently measure the accumulation of gamma emitting isotopes on the silica gel during the SIP monitoring experiments. Though our analyses of the project data are ongoing, our preliminary analyses are generally supportive of the grain (Stern layer) polarization theory of SIP.

Experiments focused on evaluating the impact of physical modifications of the medium on polarization included etching and biotic and abiotic facilitated precipitation of carbonate and iron oxides to alter the roughness and electrical conductivity of the surfaces. These experiments were performed for both silica gel and glass beads, the latter of which lacked the interior porosity and high surface area of the silica gel. The results appear to be more nuanced that the chemical modifications of the system. In general,

however, it was found that deposition of iron oxides and etching had relatively minimal or negative impacts on the polarization response of the medium, whereas carbonate coatings increased the polarization response. These results were generally consistent with changes in surface charge observed via AFM. Abiotic and biotic column flow through experiments demonstrated that precipitation of carbonate within the medium significantly impacted the real and imaginary conductivity over time in a manner generally consistent with the carbonate precipitation as observed from the batch grain coating experiments. Biotic effects were not observed to provide distinctly different signatures, but may have contributed to differences in the rate of changes observed with SIP.

AFM was used in a variety of different ways to investigate the grain surfaces throughout the course of the project. Standard imaging methods were used to evaluate surface roughness and charge density, which showed that these data could provide qualitative insights about consistency between surface trends and the electrical behavior at the column scale (for the case of glass beads). Polarization and conductive force microscopy (PCFM) measurements were developed by the original project PI (Treavor Kendall), which illustrated the importance of the initial few monolayers of water on the mineral surface for producing surface conductivity. The technique allowed for initial local estimates of complex electrical conductivity on mineral surfaces, but could not be pursued after Kendall left the project due to phase locking limitations with the AFM instrument at Clemson and an inability to perform measurements in solution, which limited their value for linking the measurements to column-scale SIP responses. As a result, co-PI Dean developed a new methodology for making AFM measurements within an externally applied electric field. In this method, the charged tip of an AFM probe is brought within the proximity of a polarization domain while an external electric field is applied to the sample. The premise of the approach is that the tip will be attracted to or rebound from charge accumulations on the surface, which allow for detection of the local polarization response. Initial experiments showed promise in terms of the general trends of responses observed, though we have not yet been able to develop a quantitative interpretation technique that can be applied to predicting column scale responses.

2. Project Results

The experiments performed in this project were focused on identifying mechanisms contributing to the complex conductivity of porous media, with an emphasis on evaluating how biogeochemical processes acting on the pore-scale environment might affect the response. Column-scale spectral induced polarization (SIP) measurements were used to measure the aggregate electrical properties of a porous medium. The project took a unique approach to directly measuring surface electrical properties at the grain scale using atomic force microscopy (AFM). This report outlines the results of the SIP and AFM measurements in two different sections.

2.1 Column-Scale Spectral Induced Polarization (SIP) Measurements

Two types of experiments were performed for the SIP measurements. The first type of experiment varied the chemical properties of the pore fluid, which in turn controls surface sorption. The second type of experiment varied the physical properties of the pore space by etching the grains or adding precipitates. In all cases, the methods followed for the SIP measurements followed the basic procedures described below.

2.1.1 Overview of SIP Methods

The general setup of all SIP experiments followed the general setup show in Figure 1. The spectral induced polarization measurements of both phase and amplitude were made with a dynamic signal

analyzer (National Instrument 4461) operated over the frequency range of 0.01-1000Hz (note the frequency range was varied for some experiments). Both current injection and potential measurement electrodes were made from non-polarizing silver wires (~Gauge 12) coated with silver chloride. Most experiments reported here were performed using a column with a length of 4.5cm and an inner diameter 2.54cm. The setup was a design used by co-PI Ntarlagiannis in other projects where the sample column fit between two blocks containing fluid reservoirs that provided electrical contact between the electrodes and sample. The advantage of the design is that many samples can be measured without the need for repacking the column (i.e., the portion of the column with the sample can be switched out). Some of the earlier measurements in the project were also measured with a more traditional column design where the electrodes were in physical contact with the sample, but significant differences in results between the columns were not noted.

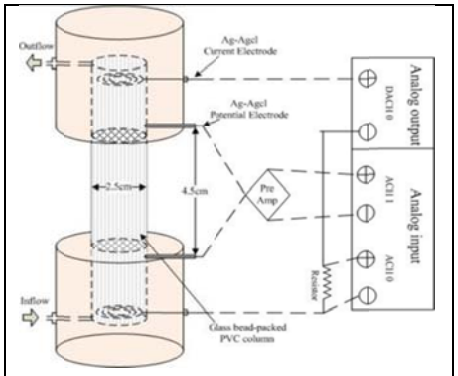

Figure 1: Schematic of the column-scale SIP measurement setup using a NI4461 Dynamic Signal Analyzer.

Prior to packing a sample in the column, the test material was typically presoaked in the measurement solution and degassed under vacuum for at least 12 hours. The test samples were subsequently carefully wet packed in the column to make sure the column was saturated without air bubbles. The influent was introduced to the column from the bottom of the column using a peristaltic pump. Data from the SIP phase and amplitude measurements were saved in text files and processed in Excel to obtain real and imaginary conductivity values. The inflow and outflow fluid conductivity and pH were measured directly in aliquots of influent and effluent using standard lab electrodes.

Prior to initiating the SIP measurement of the samples, a series of calibration tests were completed. The results in Figure 2 illustrate the level of accuracy that could be obtained, i.e., errors of below 0.02μS/cm are expected for the imaginary conductivity. Figure 2 also shows that consistent measurements could be obtained between the two different column designs used in the project.

2.1.2 – Experiments Chemically Modifying the Grain Surface

Two types of experiments were conducted to chemically modify the grain surface. First, the influence of surface sorption effects were evaluated by ion exchange experiments at a fixed surface site density. Second, the pH of the influent solution was altered to vary the surface site density under a fixed ionic composition. The chemical modification experiments were all performed using 250-500μm silica gel (Sigma-Aldrich, Grade 636) with an intragranular porosity of 38%, giving it a total surface area of 480 m^2/g; the internal pore diameter of the grains is approximately 60 Å. Silica gel was used for these experiments because the high surface area allowed for better signals of the surface processes being evaluated to be measured.

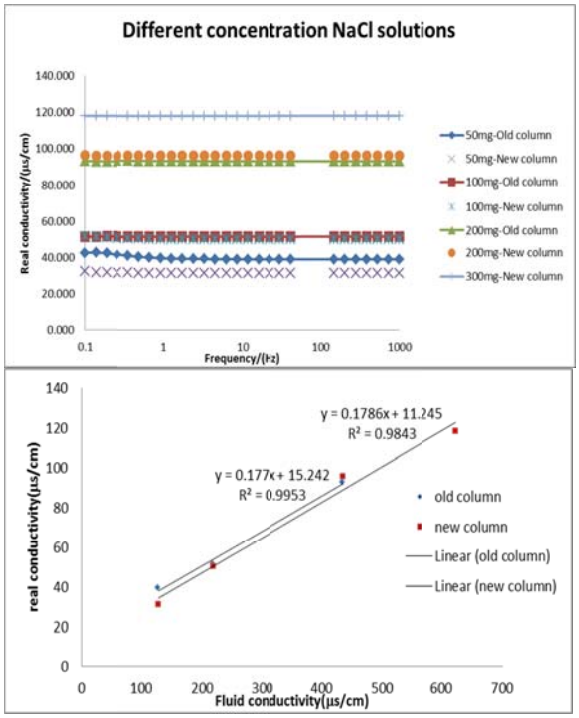

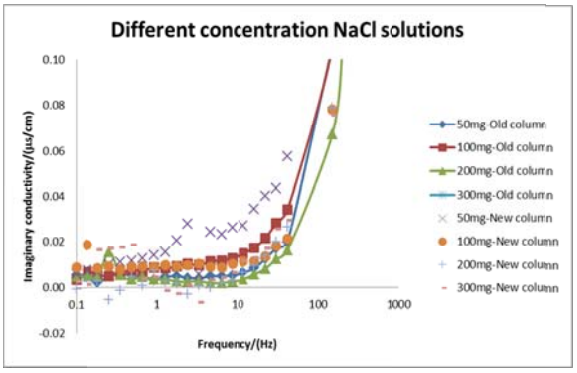

Figure 2: Calibration experiments showing real and imaginary conductivity of fluid filled the columns used in the project (left and right above). The results show that a stable and consistent reading could be obtained with both columns with an error level less than 0.02μS/cm. The plot on the bottom left shows that the two columns have a similar overall performance and geometric factor.

2.2.2.1 Na-Ca Exchange Experiments

The ion exchange experiments were performed to evaluate how complex conductivity of the medium changes as a function of the type of ion adsorbed to the mineral surface. The influent was fixed to a pH of 7 for these experiments such that the surface density of exchange sites was fixed throughout the experiment. The column was prepared by initially packing it with silica gel within a 20mM NaCl solution with a fluid conductivity of 2.81mS/cm. After collecting the SIP measurement, the column pore fluid was exchanged by pumping a 20mM $CaCl_2$ solution with fluid conductivity of 4.77mS/cm through the column at 25mL/hr for one day (equivalent to about 6 pore volumes of the column). Note that the ratio of the conductivity of the $CaCl_2$ to the NaCl solution was 1.70. This procedure was repeated on subsequent days by switching between these influent solutions, with the exception of day 6 where the concentration of the influent $CaCl_2$ was reduced to 15mM to match the fluid conductivity of the NaCl influent solution.

The results in Figure 3 show that the changes in complex conductivity of the column were consistent and reversible throughout the experiment. The real conductivity of the column increased as the NaCl solution was exchanged with $CaCl_2$. The average ratio of real conductivity of the column containing $CaCl_2$ versus that containing NaCl is 1.52±0.02 (N=5), which is consistent with, but about 12% lower than, the ratio of the influent pore fluid conductivities. In contrast, the imaginary conductivity of the column decreased by a factor of 2.50±0.07 (N=5) as the NaCl was replaced by $CaCl_2$, excluding the case when the imaginary conductivity was decreased by a slightly smaller factor of 2.18 (N=2).

The real conductivity responded to the fluid composition and concentration changes as expected. The imaginary conductivity results, however, were sensitive to the fluid composition, but not the concentration of the pore fluid. These results suggest that the number of sorption sites (i.e., negatively changed silanol groups) is the controlling factor in determining the imaginary response. Furthermore, the decrease of the imaginary conductivity for the $CaCl_2$ solution suggests a decreased mobility of Ca^{2+} relative to Na^{+} on the silica gel surface, which is consistent with stronger sorption of this ion on the surface.

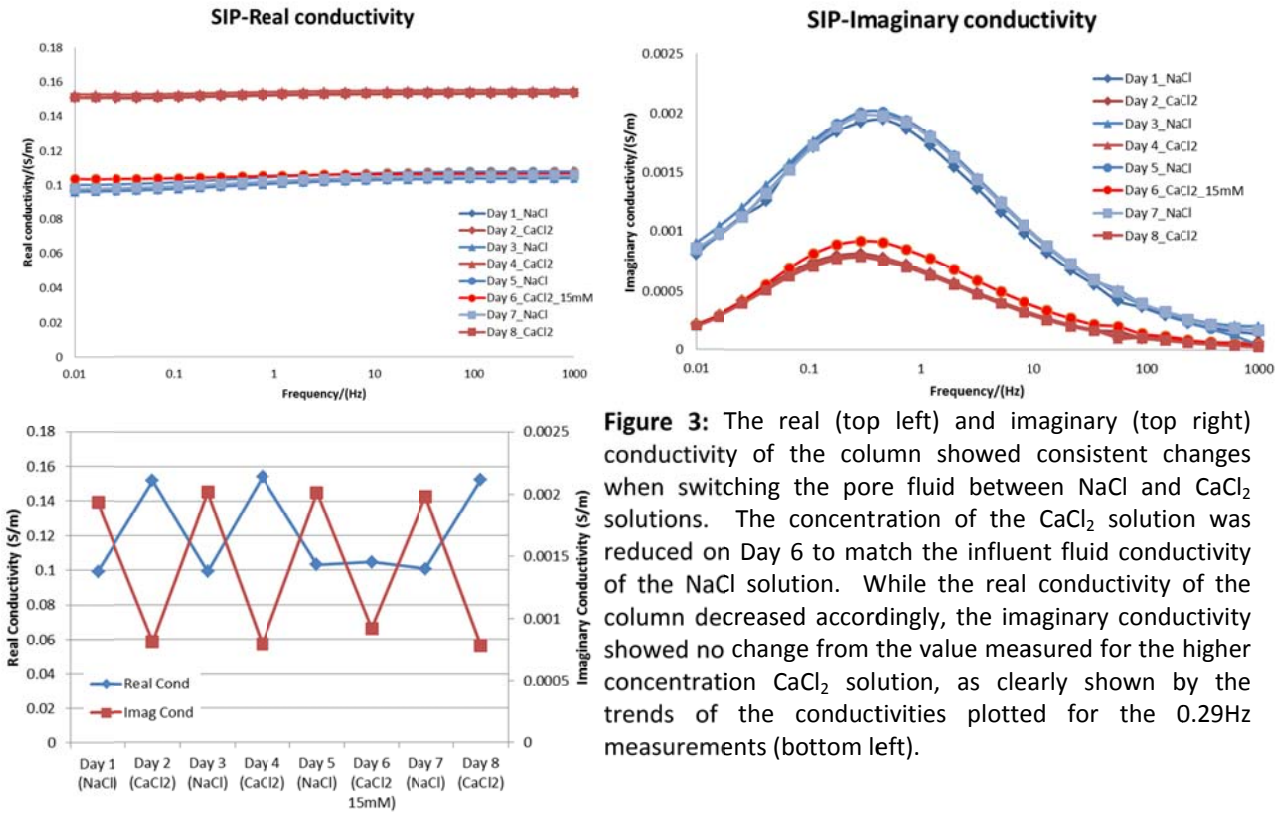

Figure 3: The real (top left) and imaginary (top right) conductivity of the column showed consistent changes when switching the pore fluid between NaCl and $CaCl_2$ solutions. The concentration of the $CaCl_2$ solution was reduced on Day 6 to match the influent fluid conductivity of the NaCl solution. While the real conductivity of the column decreased accordingly, the imaginary conductivity showed no change from the value measured for the higher concentration $CaCl_2$ solution, as clearly shown by the trends of the conductivities plotted for the 0.29Hz measurements (bottom left).

Figure 4: Electrical conductivity of the influent solution throughout the ion exchange experiment. Note the consistency relative to the real conductivity of the column.

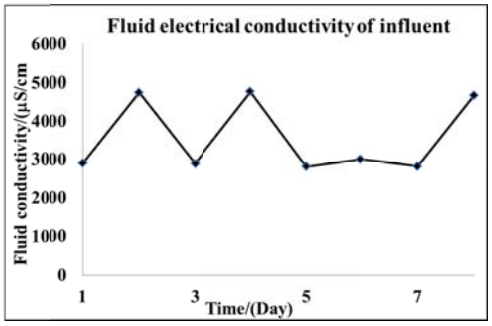

2.2.2.2 pH Control of Surface Site Density

The density of surface sites available for cation sorption on silica gel is primarily related to the deprotonation of silanol groups. If polarization of the Stern layer is a primary contribution to the imaginary conductivity, the pH of the pore fluid is therefore expected to be an important control. We performed experiments at a fixed NaCl concentration by varying the pH of the influent solution to a test column over time to evaluate this effect.

In the experiments a 50mM NaCl solution was continuously pumped through the column. The pH of the influent solution was varied over time. Figure 5 shows how the influent pH was changed for two different experiments (SG2b and SG2c) discussed in this report. SIP measurements were taken throughout the experiment and the pH and electrical conductivity of the inflow and outflow were recorded.

Figure 6 shows the change in complex conductivity observed for the column in experiment SG2b as a function of time. There is a modest (~50%) increase in real conductivity as the pH increases. The imaginary conductivity increases to a much greater degree, however, which is consistent with sorption of sodium on the surface as deprotonation of the surface increases the number of surface negatively charged surface sites. Though the influent pH was 10, the maximum pH of the effluent solution was only 8.6. The difference between influent and effluent pH indicates a substantial buffering capacity within the column. Figure 6 shows a qualitatively consistent trend between the effluent pH, which we use as an indicator of the progress toward the equilibrium deprotonation of the surface sites, and the maximum value of the imaginary conductivity observed throughout the course of the experiment (R^2=0.60).

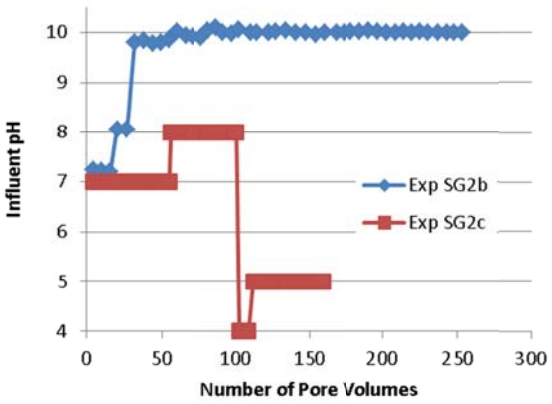

Figure 5: Record of influent pH to column for experiment SG2b and SG2c evaluating the impact of changes in pH on surface site density.

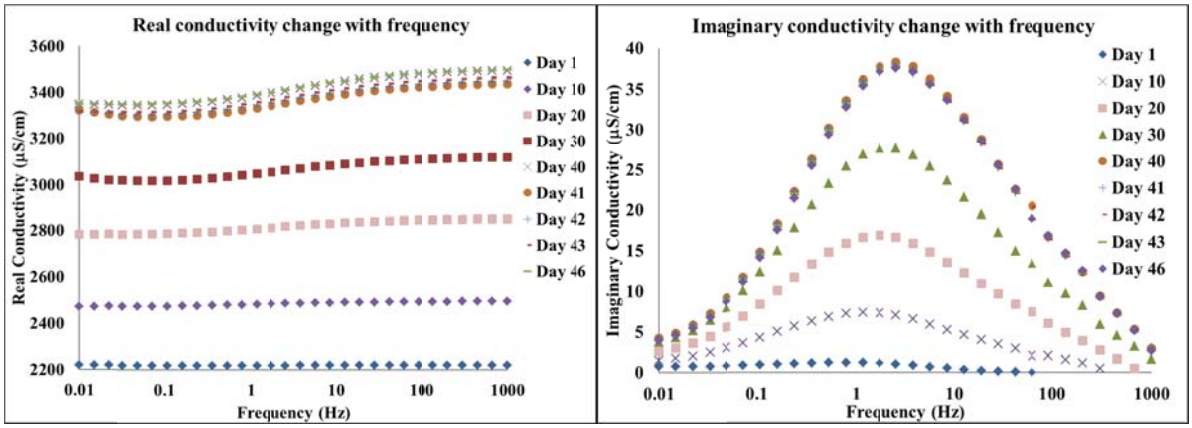

Figure 6: Real (left) and imaginary (right) conductivity measured as function of time during experiment SG2b, where the pH was increased from 7 to 10 over the course of 46 days.

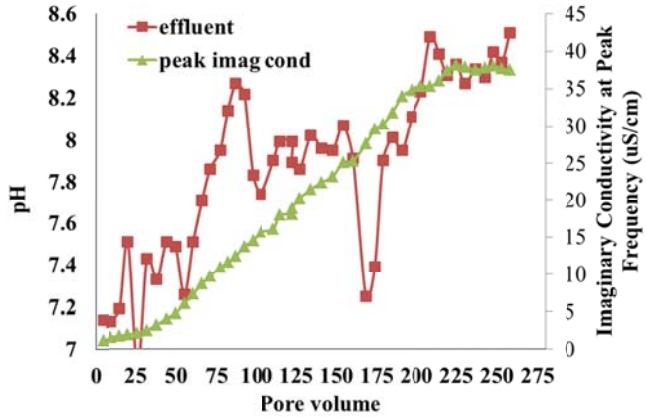

Figure 7: Correlation between changes in the pH of the column effluent and the maximum value of the measured imaginary conductivity spectrum over the course of experiment SG2b.

The first experiment (SG2b) only examined the influence of increasing pH, so another experiment (Exp SG2c) was performed where the pH was first increased and then lowered (Figure 5) to evaluate the reversibility of pH effects on the electrical behavior of the column. Figure 8a shows the change in imaginary conductivity spectra over the course of this experiment. It is apparent that the conductivity first increases as the pH is raised during the first 100 influent pore volumes where the solution is above 7, but then decreases as the pH is subsequently reduced. Figure 8b shows that the change in pH and imaginary conductivity are again consistent. The correlation between pH and imaginary conductivity is R^2=0.72 during the period when the pH is increased (first 100 pore volumes) and R^2=0.61 as the pH is lowered (Figure 8c).

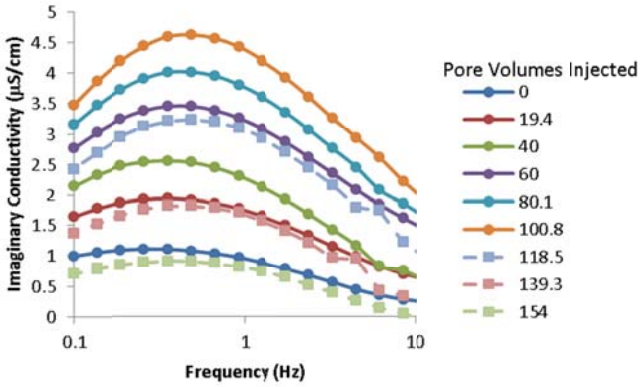

Figure 8: Evaluation of reversibility of pH influence on surface sorption (Exp SG2c). The magnitude of the imaginary conductivity spectrum increases and then decreases as the pH of the influent solution is similarly modified. A qualitative correlation is observed between the change in imaginary conductivity and effluent pH suggesting a close degree of control between pH and the imaginary conductivity response, likely through changes in the number of deprotonated silanol sites on the surface.

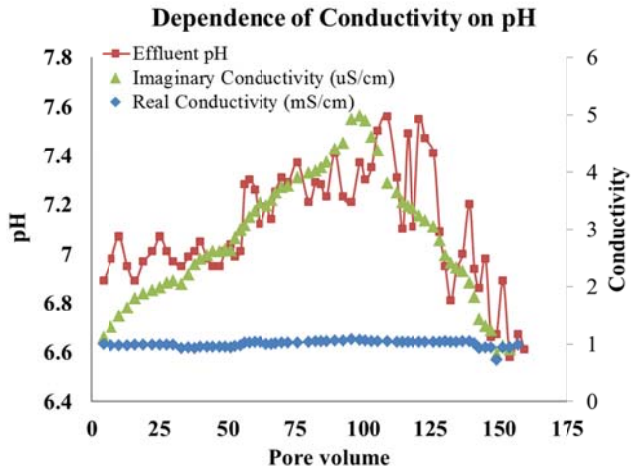

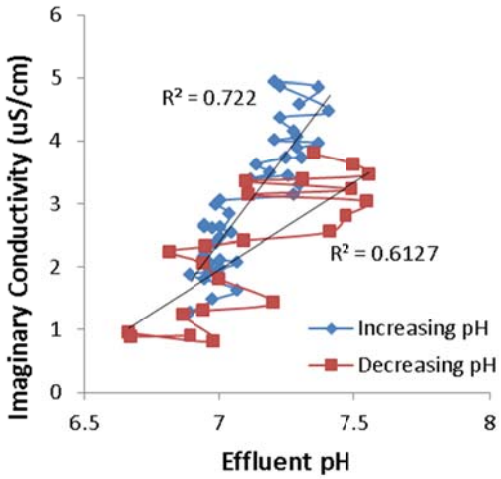

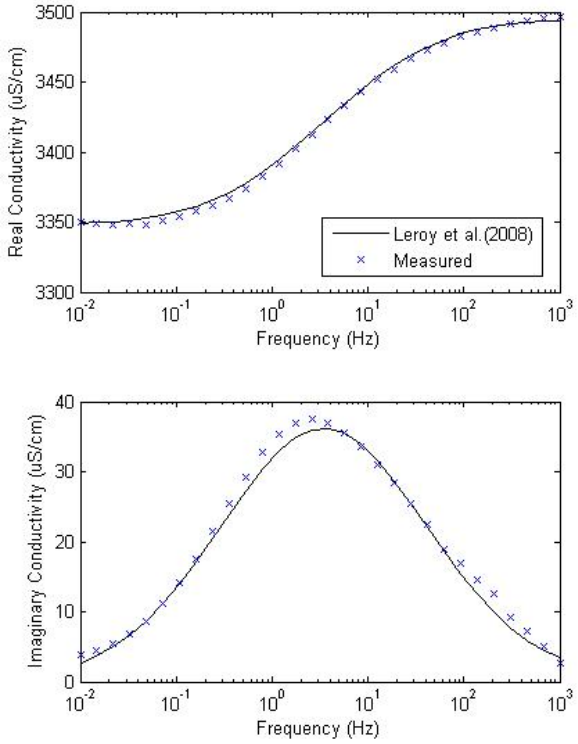

Figure 9: Example of initial fitting of SIP data by the Leroy et al. (2008) model. The data shown are from the final measurement in Experiment SG2b (pH=8.6).

Our approach to analyzing the data has so far been based on fitting the complex conductivity spectra using the mechanistic model for SIP proposed by Leroy et al. (2008). Our initial attempts at fitting the model have used an Markov chain Monte Carlo (McMC) approach to estimate four basic parameters of the model: (i) density of Na^+ sorption sites in the Stern layer, (ii) density of Na^+ in the diffuse layer, and the (iii) mean and (iv) variance of the grain size, assuming a log-normal distribution. We have also explored using a bimodal distribution to account for small pores within the silica gel, but have so far found it unnecessary to include these extra parameters to fit the data. The remaining model parameters were fixed to representative values for silica, water, and sodium ions. The initial results of the model fit are shown for one example data set in Figure 9 and the parameters for this model are given in Table 1. The estimated grain size distribution (Figure 10) appears to be reasonable given the manufacturer's specifications for the silica gel, particularly when considering that the small internal pores are expected to provide a significant contribution to the total surface area of the silica gel and, therefore, to the SIP signal.

To evaluate the validity of the site density values estimated for the triple layer model, we performed independent acid-base titrations of the silica gel as a function of pH. These potentiometric titrations were performed with a NaCl solution at four different ionic strengths (0.02, 0.03, 0.05, 0.2M) in the pH range 5-10. In addition to the chemical titration and analysis, we used numerical code FITEQL to fit the titration results with triple layer model. The results of the titration experiments and FITEQL results are shown in Figures 11 and 12. The estimated surface site densities for the Stern and diffuse layers under conditions similar to the final measurement time of the SIP experiment (i.e., pH=8.6) are given in Table 1. Comparison of the titration and SIP results indicates that the surface site densities appear to be greatly overestimated. It is currently unclear whether this difference is a results of inadequacy of the SIP model, the data fitting, or a difference between the two measurement methods. The last issue could be

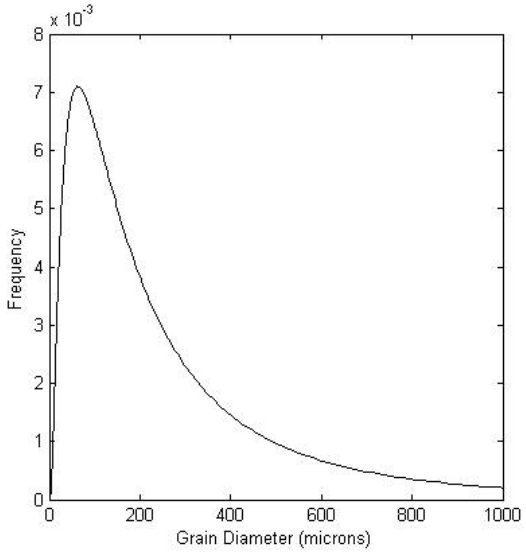

Figure 10: Grain (pore) size distribution of silica gel estimated from inversion of the SIP data.

significant given that the time taken for the automated titration experiments is significantly shorter than that for the SIP experiments. As a result, there is sufficient time for ions to migrate within the interior of the silica gel during the SIP measurements as the grains are exposed to the pore fluid for days, whereas this may not be possible for the titrations which take only minutes. We are planning to continue experiments varying the inflow rate to the SIP column to evaluate the significance of diffusion within our results. An alternative explanation could also be related to unaccounted for mechanisms in the Leroy et al. (2008) model that significantly contribute the SIP signal, such as the proposed proton hopping mechanism discussed recently by Skold et al. (2013).

Table 1: Comparison of Estimated and Expected Parameter Values for the SIP Model

Parameter	SIP Estimated Value	Expected Value*
Grain radius mean	31.6×10^{-6} m	100×10^{-6} m
Grain radius st. dev.	51.0×10^{-6} m	N/A
Stern layer site density	6.66×10^{17} sites/m^2	2.6×10^{15} sites/m^2
Diffuse layer site density	8.05×10^{18} sites/m^2	1.64×10^{17} sites/m^2

*Expected values are based on the manufacturer's specifications for grain size and the titration results for the site density.

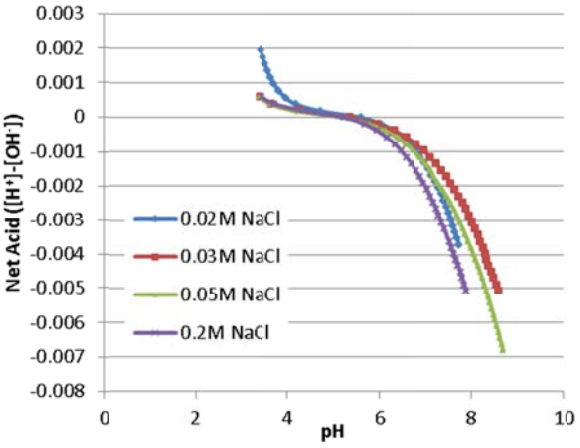

Figure 11: Results for base titration of silica gel at salt concentrations from 0.02-0.2M.

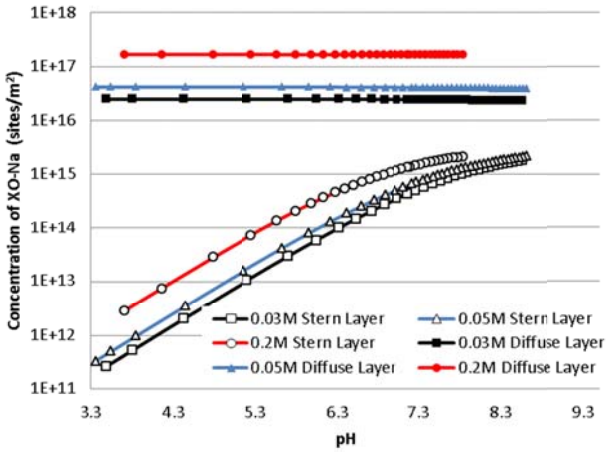

Figure 12: Surface site density as a function of pH for the Stern and diffuse layers based on fitting the triple layer model with the acid-base titration data using Fiteql.

2.2.2.3 Direct Evaluation of Surface Sorption using Na-22

The uncertainties associated with the interpretation of the SIP experiments above are related to a poor understanding of what ions are actually present on the grain surface. As an extension of this project, we are currently repeating the pH variation experiments described above while undertaking additional measurements that will allow us to directly measure the accumulation of sodium ions on the silica gel surface. Specifically, we will add a spike of radioactive Na-22 to the influent solution as we alter the pH. We expect that we will be able to use gamma counting to detect the accumulation of the radioactive sodium on the surface as silanol groups are deprotonated. Preliminary measurements that we have performed as batch experiments (Figure 13) illustrate that we expect to have sufficient sensitivity to detect the Na-22 as it accumulates, therefore providing a direct measure of ion density on the silica gel surface during the SIP measurements.

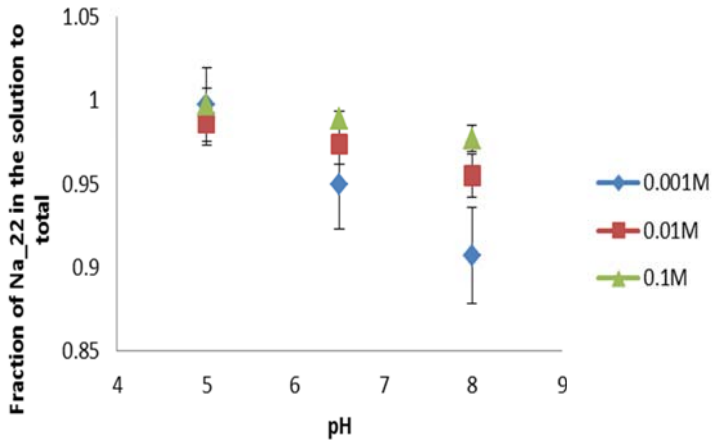

Figure 13: Measured fraction of Na-22 sorbed to silica gel as a function of pH for solutions with different NaCl concentrations. Based on these results, we expect that we should be able to measure a 5-10% increase in activity associated with Na-22 sorption as the pH of the influent to SIP column is increased.

2.1.3 – Experiments Physically Modifying the Grain Surface

We focused on three different types of treatments to modify the grain surface of silica gel and glass beads. Glass beads were used in addition to the silica gel for these experiments so that effects related to pore spaces and external surfaces could be isolated from those associated with the internal micropores that contribute to the high surface area of the silica gel. To increase the roughness of the grain without affecting the chemical composition, we used hydrofluoric acid to etch the surfaces. In contrast, we used coatings and direct precipitation of carbonate particles and amorphous iron oxides to affect surface roughness, composition, and also potentially constrict pore spaces and throats.

Figure 14: SEM images showing untreated, etched, and iron oxide coated glass beads and silica gel.

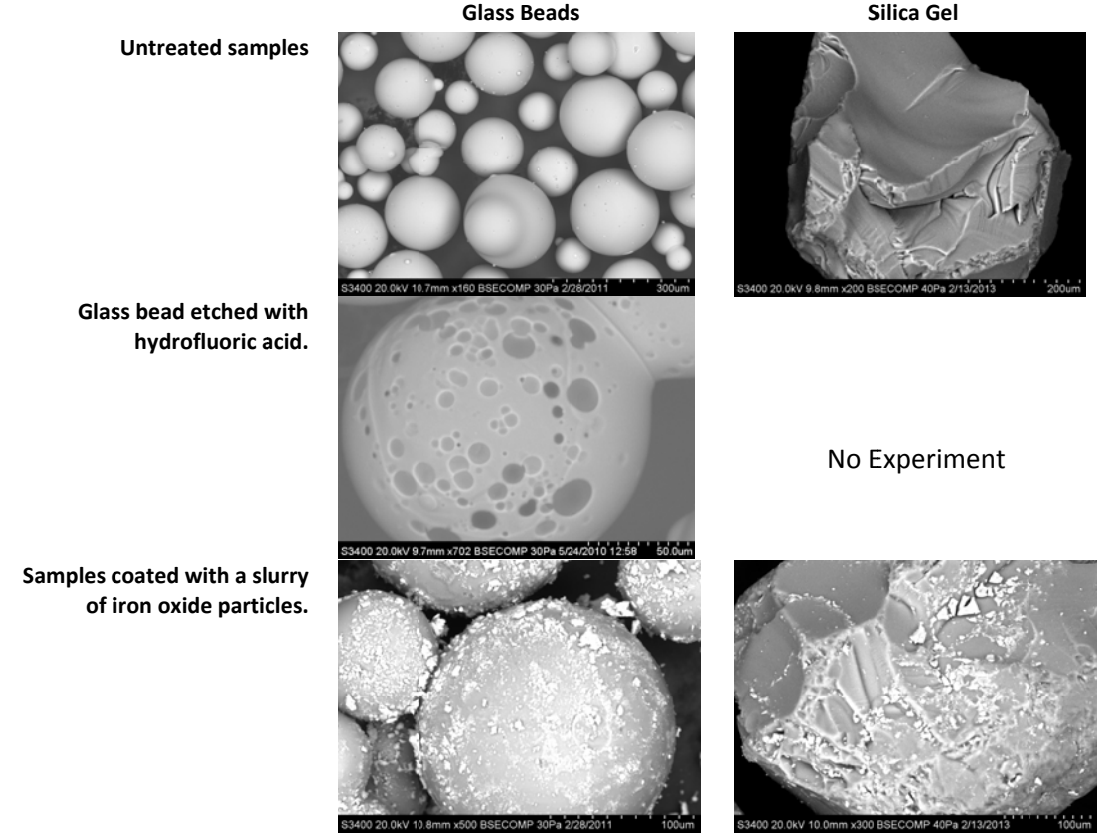

Figure 15: SEM images showing results of different carbonate treatments for glass beads and silica gel.

Glass beads coated with calcite precipitated from solution

Silica gel coated with fresh calcite crystals

Silica gel coated with a slurry of commercially prepared calcite powder

Silica gel with calcite coating precipitated on surface from solution by evaporation

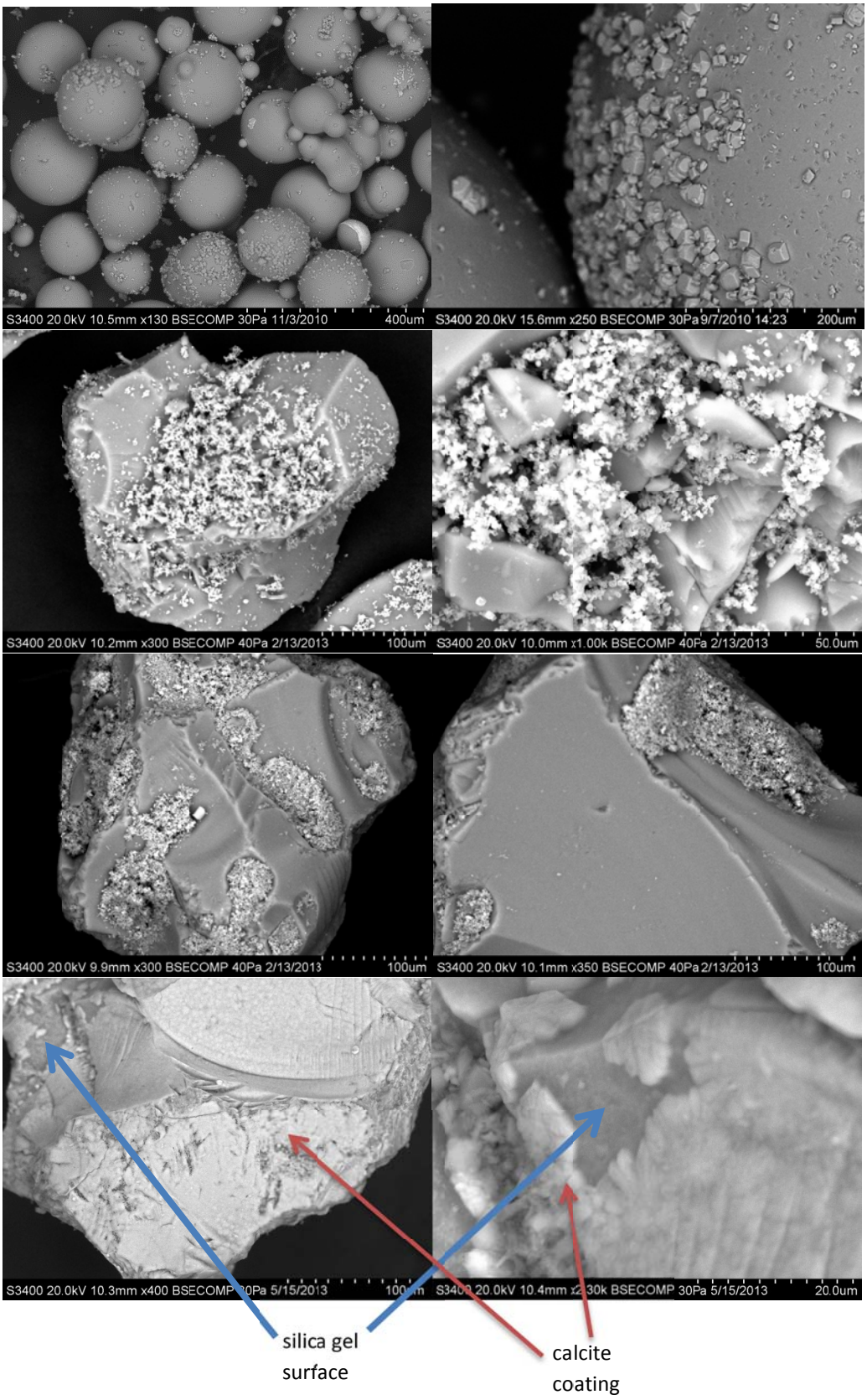

The SEM images in Figure 14 and 15 illustrate that the surface treatments were successful. The iron oxide coatings were obtained by using a slurry of iron oxide particles to coat the grains. A similar approach was used to coat the silica gel with pre-prepared calcite particles; we used freshly prepared crystals and commercial calcite powder to evaluate potential effects of carbonate aging. From the SEM images it is clear that the form and distribution of particles is somewhat different in these two cases. In contrast, we precipitated calcite directly on the surface of the silica gel by placing the sample in a saturated solution of calcium carbonate that was allowed to evaporate. In this case, we were able to produce a continuous sheet of precipitate; our goal was to use the precipitate to partially seal the interior pore space. The glass beads were coated by allowing the crystals to form directly on the grain surface, either in batch preparation or during column experiments.

Independent measurements of surface area were performed using the BET method for nitrogen adsorption isotherms. The results of the measurements are shown in Table 2. A small reduction in surface area (7%) occurred for the iron oxide coated sample relative to the untreated silica gel, indicating that the iron oxide didn't significantly add to or reduce the overall surface area of the sample. In contrast, the case where calcite was precipitated as a continuous sheet on the silica gel surface reduced the surface area by 46%, suggesting that access to the interior pores of the silica gel was partially blocked. To a lesser extent, coating the silica gel with calcite particles also led to an overall reduction of surface area, but only by about 30%.

Table 2: Surface area (m^2/g) silica gel estimated by nitrogen adsorption (BET)

Treatment	1st sample	2nd sample(replicates)
Untreated silica gel	515.68 ± 1.78	507.34 ± 1.01
Iron oxide coated	487.33 ± 1.84	468.47 ± 1.88
Calcite precipitated on surface from solution	286.78 ± 0.95	265.76 ± 1.00
Coated with fresh calcite particles	357.86 ± 1.24	339.20 ± 1.34
Coated with commercial calcite particles	380.15 ± 1.34	381.91 ± 1.44

2.1.3.1 Results for Physical Modification Experiments with Glass Beads

Each of the different treatments were applied to the glass beads prior to packing each sample in the column. Figure 16 shows some of our initial experiments evaluating the effect of etching the grain surface (Exp GB2a). The results suggested that the etching had a significant effect on the SIP response, nearly doubling the imaginary conductivity. These initial measurements were performed, however, while packing the beads in the column without flow (i.e., dry packing). Given concerns over air entrapment, shortly after these initial experiments we switched to wet packing methods using samples that had subsequently been placed under vacuum for at least 12 hours to reduce the potential for air entrapment within the sample. Figure 17 shows the results for three independently packed columns of 200μm diameter etched glass beads in a 100mg/L solution of NaCl under neutral pH (Exp GB2f). From these measurements it appeared as though the etching likely had no effect on the grains and that the air entrapment due to dry packing of the column affected the results, causing an apparent increase in response. Since air entrapment was not a variable that could be controlled experimentally in our work, we used wet packing for all future experiments. To confirm the response observed in experiment GB2f, we repeated the etching experiments once more for two replicate, independently prepared columns with the wet packing methods (Exp GB2g) and again found no apparent difference between the control sample of glass beads versus the etched grains (Figure 18).

Figure 16: Initial experiments comparing etched glass beads to a control sample under different NaCl solution concentrations. The sample was prepared using dry packing methods. (Exp GB2a)

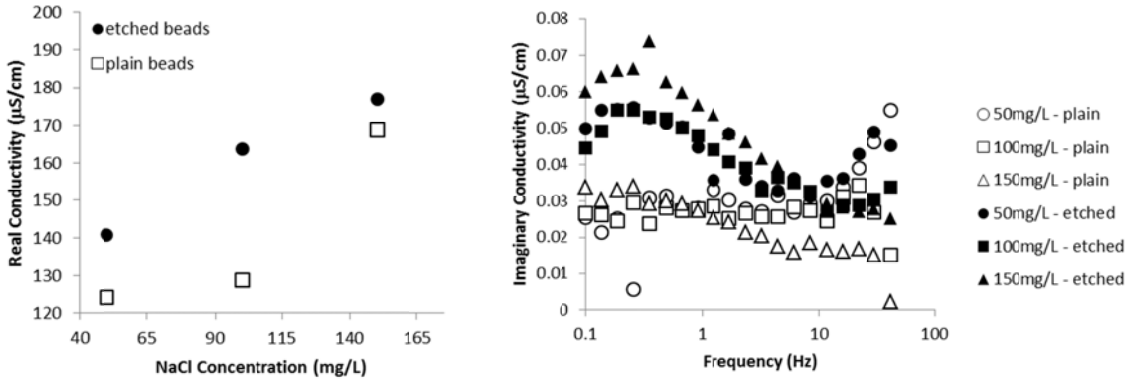

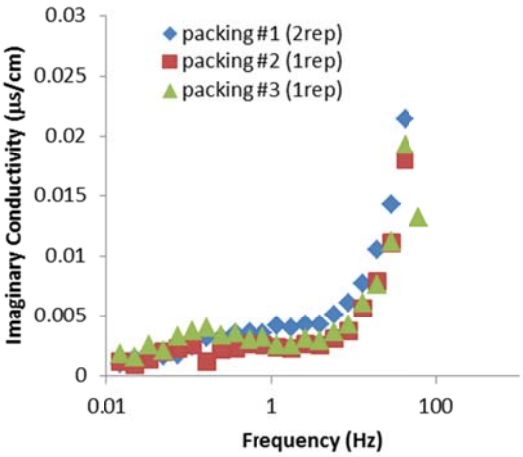

Figure 17: Imaginary response of etched glass beads carefully prepared with wet packing methods to avoid air entrapment within the column. (Exp GB2f)

Figure 18: SIP results for glass beads. Note the minor change in real conductivity and lack of polarization response for the samples. (Exp GB2g - etched beads; Exp GB4g – iron oxide coated beads)

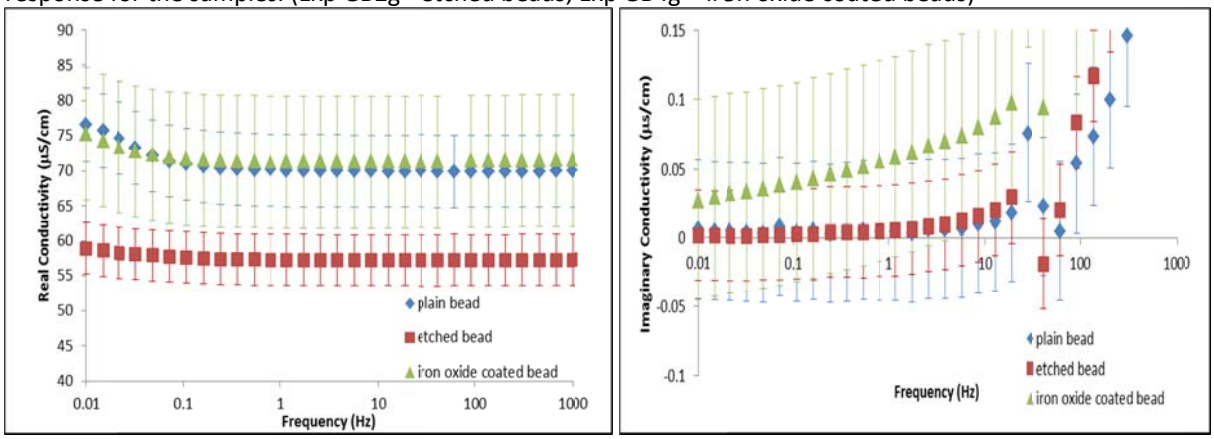

Figure 18 shows a summary comparing the results of SIP measurements made using the glass beads for the etching and iron oxide coating treatments. The experiments were performed using 200micron diameter beads in a NaCl solution with fluid conductivity of 212µS/cm and neutral pH (uncontrolled). The measurements show the average result of two replicate measurements made in two separately packed columns, i.e., the effect of packing variability is accounted for. The results suggest no significant

change in real conductivity for the iron oxide coated bead relative to the untreated bead, whereas a small, but significant decrease in conductivity for the etched bead. The reduction in real conductivity could possibly be related to an increase in surface roughness for the etched grains. In contrast, no detectable polarization response was measured by the imaginary conductivity of the samples at frequencies below a frequency of 10 Hz. There was a small increase in the observed imaginary conductivity for the iron oxide grains observed in multiple experiments, but the effect wasn't large enough compared to the variability in the replicate measurements to justify interpretation. In general, the measurements made on the glass beads were near or below the expected accuracy of the SIP measurements.

2.1.3.2 Results for Physical Modification Experiments with Silica Gel

The experiments described above for physical modification of the glass bead surface were repeated for the silica gel in a NaCl solution (0.01M, pH=7.29, 119.3mS/cm). The silica gel has a significantly larger polarization response than the glass beads (Figure 17), thereby allowing for better comparisons to be made for how the treatments may increase or decrease the complex conductivity response. Given the complex pore structure and surface geometry of the silica gel, we did not perform etching experiments for this material, but we did compare the influence of iron oxide and calcium carbonate coatings on the silica gel. Different types of carbonate coatings were compared to evaluate (i) the influence of carbonate aging on the response, and (ii) effects associated with coatings formed with discrete particles versus a continuous layer of calcite on the surface.

We found that the iron oxide coatings decreased the imaginary conductivity of the silica gel, but had little to no effect on the real conductivity (note the response to glass beads is shown for comparison). This is in contrast to the effect observed for glass beads, where the iron oxides caused either no response or possibly a small increase in the imaginary conductivity. Independent surface area measurements showed only a small difference (7%) between the iron oxide coated and treated silica gel (Table 2), thus no effects related to a change in surface area are expected. AFM measurements of the iron oxide material (discussed later in this report) also suggested no change in fixed surface charge relative to an untreated silica surface, suggesting that the iron oxides may have minimal impact on SIP response other than through pore blockage. Given that we expect the iron oxides to be electrically conductive, however, it is possible that the addition of this material to the silica gel allowed for some bridging of polarization domains, e.g., grains or micropores, to produce the net decrease in imaginary conductivity observed. A specific mechanism explaining the effect, however, has not yet been identified.

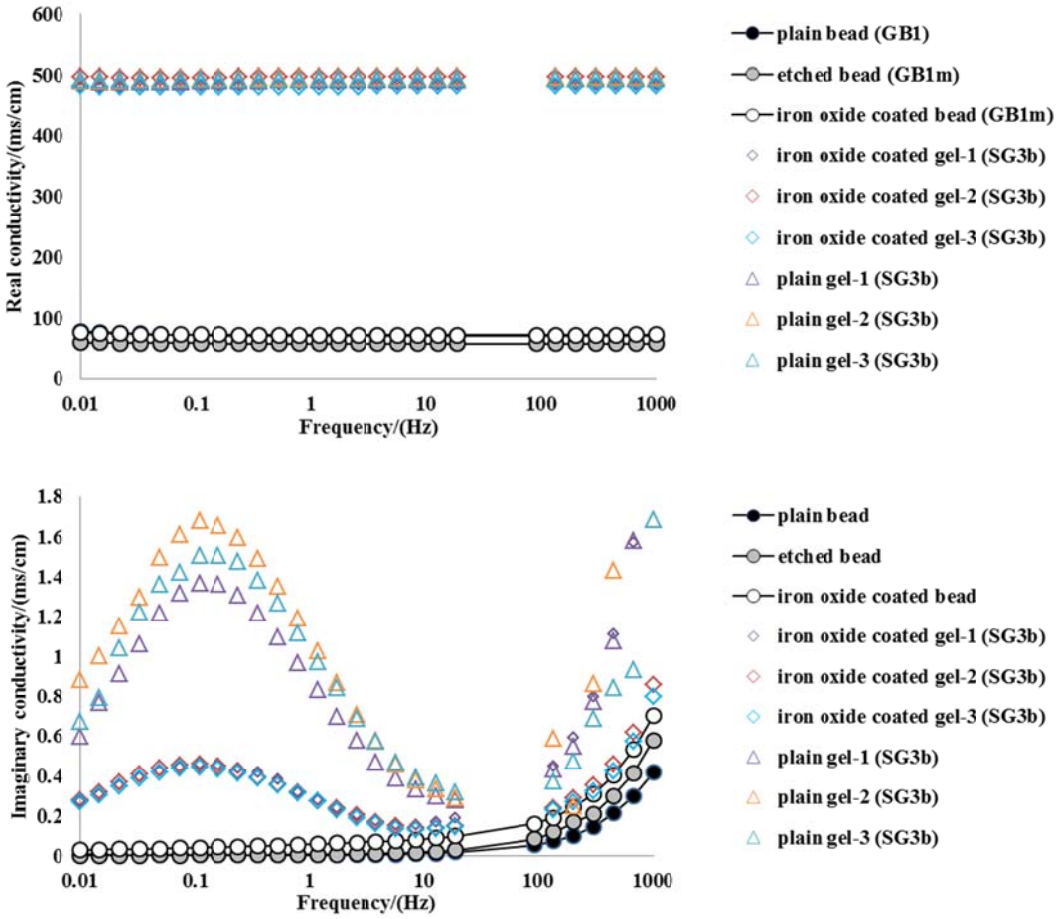

Figure 19: Influence of iron oxide coatings on the imaginary conductivity of glass beads and silica gel. Three replicate measurements from repacked columns are shown for the silica gel to illustrate the variability in the measurements, whereas the average of three independent replicate columns is shown for the glass beads to highlight the difference in the signals. (Note that the difference in real conductivity is because the glass bead measurements were performed with a 1mM NaCl pore filling solution, whereas the solution concentration was 10mM for the silica gel measurements. In other experiments not shown, the concentration did not significantly increase the imaginary response of the glass beads.)

Unlike the iron oxide coatings, we found the treatment of the silica gel with calcium carbonate coatings produced a substantial increase in the complex conductivity (Figure 20). In the particular experiment shown in Figure 20 the coatings were produced by physically mixing calcite powder slurries with the silica gel grains. Two different types of calcite powder were considered; the first was obtained as calcite powder from a commercial vendor and the second was produced by harvesting the precipitate created by mixing Na_2CO_3 and $CaCl_2$ solutions. SEM images indicate that the chemically precipitated calcite was loosely packed and widely distributed across the silica gel surface, whereas the commercial powder tended to form isolated, packed clumps (Figure 15). Despite this difference in morphology, no significant difference in surface area determined by nitrogen porosimetry was observed between the coated samples, though both had about 30% less surface area than untreated silica gel. Previous AFM measurements of the calcium carbonate precipitates suggested an increase in negative fixed surface charge relative to an untreated silica surface, thus providing a possible explanation for the observed increase SIP response.

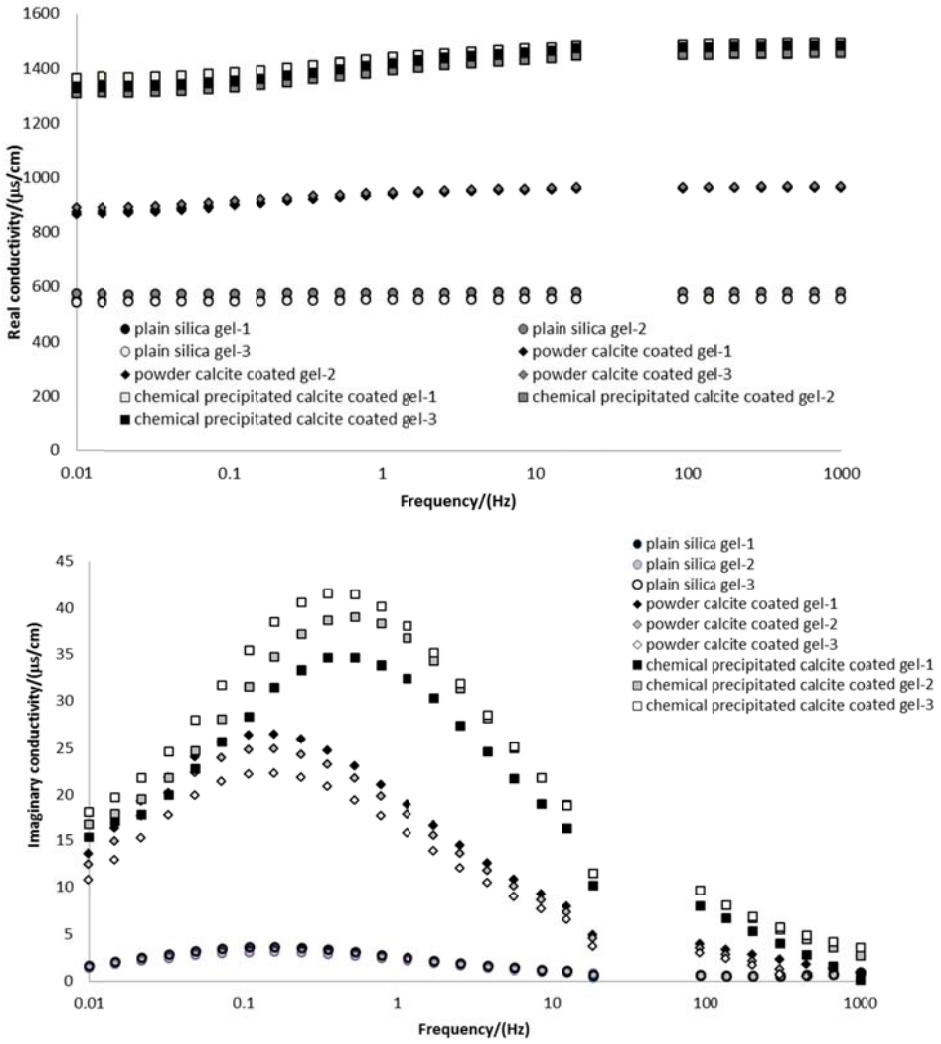

Figure 20: Influence of calcium carbonate coatings on the imaginary conductivity response of the silica gel. Note the influence of the source of the calcium carbonate coatings and the larger range of scale compared to Figure 1. Three replicate measurements from independent repacked columns are shown for each treatment.

The SIP measurements were performed on three independently packed columns in a 0.01M NaCl solution saturated with $CaCO_3$. In both cases the real and imaginary conductivity of the treated silica gel is much greater than that of the untreated control sample. The increase in real conductivity suggests that a change in the conductivity of the pore fluid may have occurred. This could be explained by local dissolution of the calcite, despite our efforts to keep the solution saturated. The smaller, more loosely packed grains of calcite observed for the "fresh" particles used in the coating would also be more likely to dissolve than the more tightly packed, "aged" particles obtained from the commercial vendor, thus potentially explaining the smaller response for the latter. The importance of the smaller disseminated calcite grains also appears to express itself as a shift in the peak frequency of the imaginary conductivity spectrum.

To further investigate the effect of the form of the calcite coating on the SIP response, we prepared samples of silica gel where carbonate phase was precipitated on the surface as a saturated $CaCO_3$ solution was evaporated (Figure 15). Our objective of encasing the silica gel grains in calcite was two fold: (i) to change the surface chemistry of the grains, and (ii) to reduce access to the interior porosity of

the silica gel grains. The SEM images along with the 46% reduction in porosity of the treated samples suggests that we were generally successful in this effort. The SIP response shown in Figure 21 indicates that the treatment cause an increase in both the real and imaginary conductivity. The magnitude of the changes roughly fell between the response observed for the other two treatments. A shift in the relaxation peak to higher frequencies was also observed in these samples, similar to the case for the sample packed with "fresh" calcite particles. Given that small calcite mineral grains are not apparent in the SEM images as they are for the particle coated sample, it is not clear that a shift in grain size is an adequate explanation for the frequency shift. Another explanation could potentially be related to an increase in the effective diffusion coefficient and ion concentration near the grain surfaces, which could be related to local carbonate dissolution. Though we were not able to directly confirm dissolution by mass balance, we did observe a substantial change in fluid conductivity when the treated samples were allowed to sit for 12 hours (initial pH=7.42 and conductivity =148mS/cm, final pH=7.02 and conductivity = 2012 mS/cm), suggesting that dissolution within the sample was an important factor.

After the completing the SIP measurements, we acidified the sample columns to remove the calcite from the surface of the sample grains. We then again measured the SIP response to confirm that the change in the real and imaginary response was indeed due only to the presence of calcite and not a change in the character or structure of the silica gel (Figure 21).

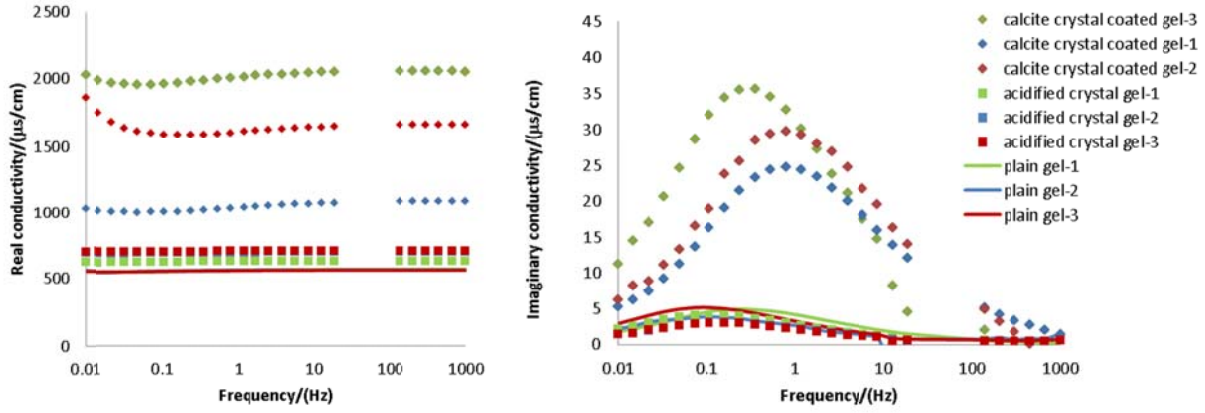

Figure 21: Complex conductivity of silica gel with a layer of calcium carbonate precipitate. After acidifying the sample, the response returns to similar values measured for control conditions.

2.1.3.3 Results for Physical Modification Experiments with Silica Gel

The results above were performed from batch experiments where grains were modified and subsequently packed into a column for SIP measurements. In most cases, SIP measurements will be used in situ for monitoring environmental changes. We therefore performed a set of column flow experiments to evaluate how dynamic changes in calcium carbonate precipitation affect the SIP response over time. By coating the samples prior to packing them in the column, the batch experiments were also designed to avoid accumulation of precipitates in pore throats. These dynamic experiments, in contrast allow for the accumulation of carbonate precipitates within the pore space. By measuring changes in the complex conductivity over time, we expected to achieve better sensitivity to small changes in response given that variability due to packing effects would not occur, so we opted to perform these experiments using the simpler geometry of the glass beads. The experiment was conducted by introducing Na_2CO_3 and $CaCl_2$solutions to the column through different inlets, then allowing the solutions to mix and precipitate $CaCO_3$ within the column.

(a) An increase in imaginary conductivity was observed in the first four hours of the inflow experiment. The increase was observed at a frequency range greater than that for the expected peak response of the glass bead.

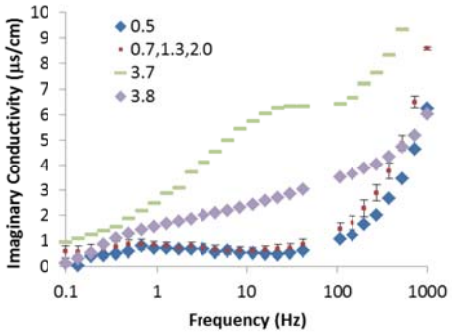

(b) The imaginary conductivity decreased to values smaller than the initial value for the remaining five days of the experiment from hours 4-139 (earlier times are shown for reference).

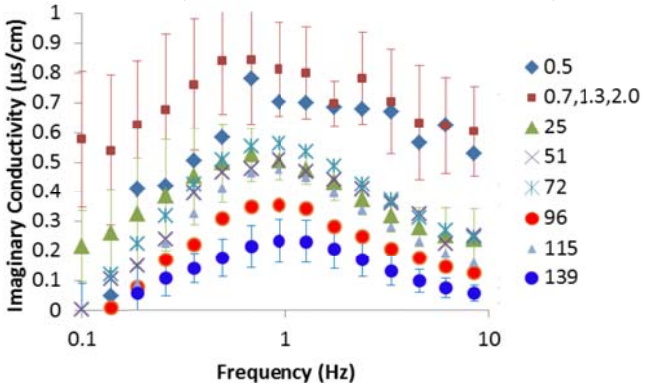

(c) Change in the real conductivity of the column relative to the conductivity and pH of the effluent fluid. Vertical error bars indicate standard deviation of values measured within the time period indicated by the horizontal error bars.

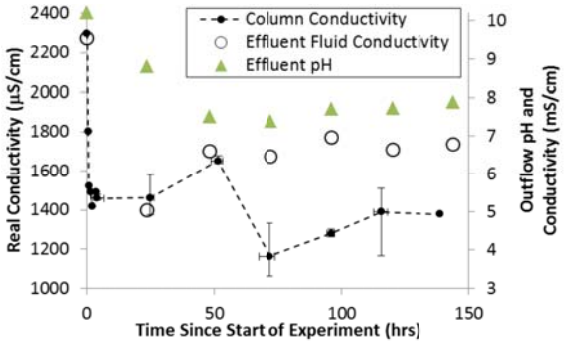

(d) Comparison of real and peak imaginary conductivity (<10Hz) over time during the experiment. An initial drop of real conductivity and sharp increase followed by a drop is observed for the imaginary conductivity.

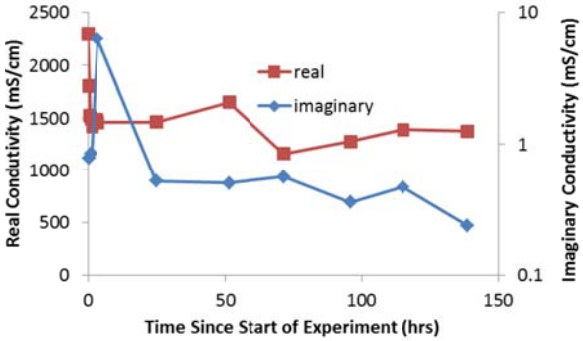

Figure 22: Time dependent changes in complex conductivity observed during the carbonate precipitation experiment. Legend values in (a) and (b) indicate the time for the measurements; data with error bars indicate the average and standard deviations for multiple measurements taken within a ~5 hour window on each day for t=25hrs and t=139hrs. (Data for Exp GB3a)

Changes in the complex conductivity of the column over the course of the carbonate precipitation experiment are shown in Figure 22. A large increase in the imaginary conductivity occurs approximately 3-4 hours after initiating mixing of the Na_2CO_3 and $CaCl_2$ solutions in the column (Figure 22a,d). By the second day of the experiment, however, the imaginary conductivity decreases to values smaller than those observed prior to t=2hrs, i.e., smaller than the initial value observed before the large spike in imaginary conductivity occured at ~3-4hrs. Over the next 5 days the magnitude of the imaginary conductivity continually decreased with time (Figure 22b,d). The real conductivity of the column drops drastically within the first hour of the experiment. This change is consistent with an observed decrease in the fluid conductivity of the column effluent (Figure 22c). The real conductivity of the column appears to match changes in fluid conductivity until about 50hrs into the experiment at which point the fluid conductivity remains stable, but the real conductivity of the column drops by about 16%. The decrease in real conductivity of the column while the fluid conductivity remains stable, suggests a loss in porosity.

Overall, the changes in complex conductivity indicate at least two different periods of behavior during the experiment. The initial onset of carbonate precipitation in the column is consistent with the high-

frequency spike in imaginary conductivity along with the drop in the real conductivity caused by loss of ions from solution. Later, the drop in real conductivity to values lower than that consistent with changes in fluid conductivity along with the continuous decrease in imaginary conductivity of the column suggest a period of carbonate accumulation associated with the closing of pore throats.

2.1.3 – Experiments Biologically Modifying the Grain Surface

One of the goals of our project was to evaluate how biologic factors might affect the SIP response. Given that biologically mediated changes in pore fluids is an important process within the pore spaces, the abiotic experiments described above provide an important reference to compare microbial responses against. To test for a difference in response between geochemically controlled and biologically mediated effects, we performed batch and flow experiments with the bacterium *Sporosarcina pasteurii*. We selected this bacterium as it is capable of mediating calcite precipitation through ureolysis, thus providing a similar geochemical conditions as the abiotic experiments above.

We were able to successfully culture the bacterium in the laboratory and performed a series of batch experiments for the calcite system consisting of biotic (bacteria, 12mM urea, and 3.5mM $CaCl_2$), abiotic (12mM urea, 3.5mM $CaCl_2$, 69mM $(NH_4)_2CO_3$), and controls (one with no bacteria, i.e., $CaCl_2$ and urea, and one with no calcium, i.e., urea and bacteria only). Our results showed decreases in the real conductivity of the biotic and abiotic samples where calcite precipitation was allowed to occur, but no change in the control samples (Figure 23). This result is consistent with removal of $CaCO_3$ from solution during precipitation. SEM imaging indicated fewer crystals formed in the biotic vs. abiotic case and suggests that the form of carbonate phase precipitated was aragonite rather than calcite (Figure 24). Both biotic and abiotic samples showed that the peak of the imaginary conductivity shifted to higher frequencies, but the signals are small and not clearly distinct from the control samples.

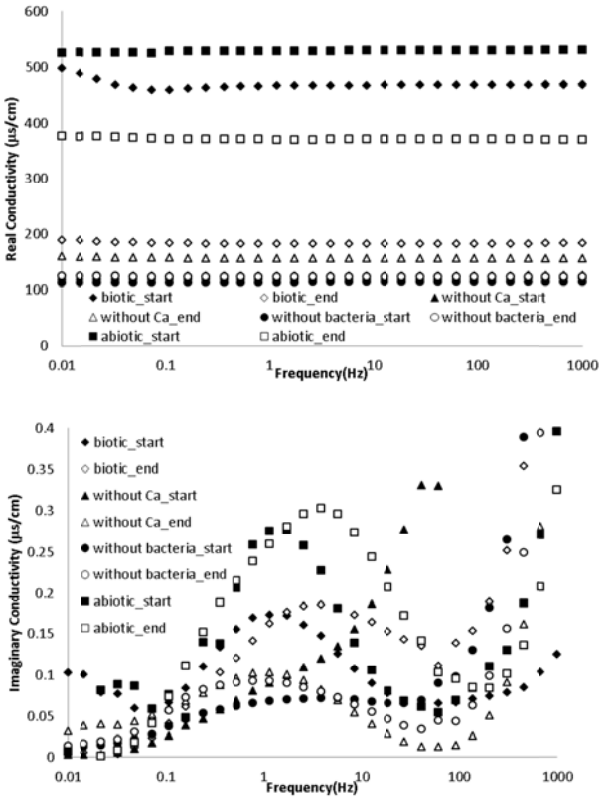

Figure 23: Comparison of SIP results for abiotic and biotic calcium carbonate precipitation in a batch experiment.

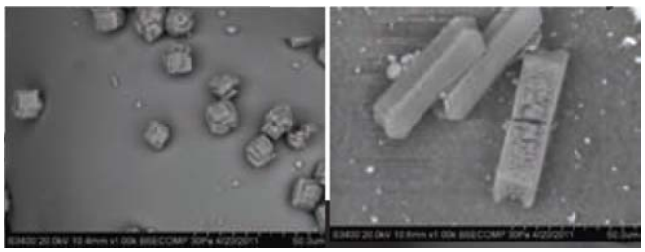

Figure 24: SEM images comparing calcium carbonate crystals formed during abiotic (left) and biologically mediated (right) precipitation.

A flow experiment parallel to the abiotic experiment described above was also performed by inoculating a column with *S. pasteurii*. The column was initially saturated with bacteria and urea solution. After the bacterial colony was established, we introduced a 0.02M $CaCl_2$ and urea (5g/L) solution to promote the precipitation of calcite within the column. The results of the experiment showed a general decrease in the real conductivity of the column until approximately 75 hours into the experiment. The decreasing real conductivity is consistent with the decreasing conductivity of the column effluent over time and the accumulation of precipitate within the column. After this time the real conductivity increased, even though the effluent conductivity continued to decrease. This response is in contrast to what was observed for the abiotic flow experiment. It is not clear if the change was caused by opening up of pore space that had been filled during the precipitation phase or if it is related to some other biotic or abiotic process occurring in the column. The imaginary conductivity was also observed to increase over time, which is also consistent with the accumulation of calcite in the column as initially observed for the abiotic experiment. Although the imaginary conductivity became temporarily unstable at 75 hours, i.e., when the real conductivity suddenly increased, it continued to increase after the transition event. SEM imaging of the precipitate after the experiment revealed a wide array of precipitate morphologies were formed in the column, including cubic crystals, amorphous globular clusters, and sheets on the grain surfaces (Figure 26). Clear evidence was also present for the formation of abundant precipitate within the pore spaces as contacts of the precipitate with grain surfaces that had been broken away when the column was destructively sampled.

Overall the impacts of biologically mediated precipitate formation appear to be similar to the observations made during abiotic precipitation, which the surface and pore-filling effects of mineral formation dominating the process. The rate at which these processes occur and how they progress over time, however, may be identifiable in SIP data. Further detailed work, e.g., including non-invasive imaging, is required to understand the intricacies of processes occurring within the columns over time to better interpret the SIP results.

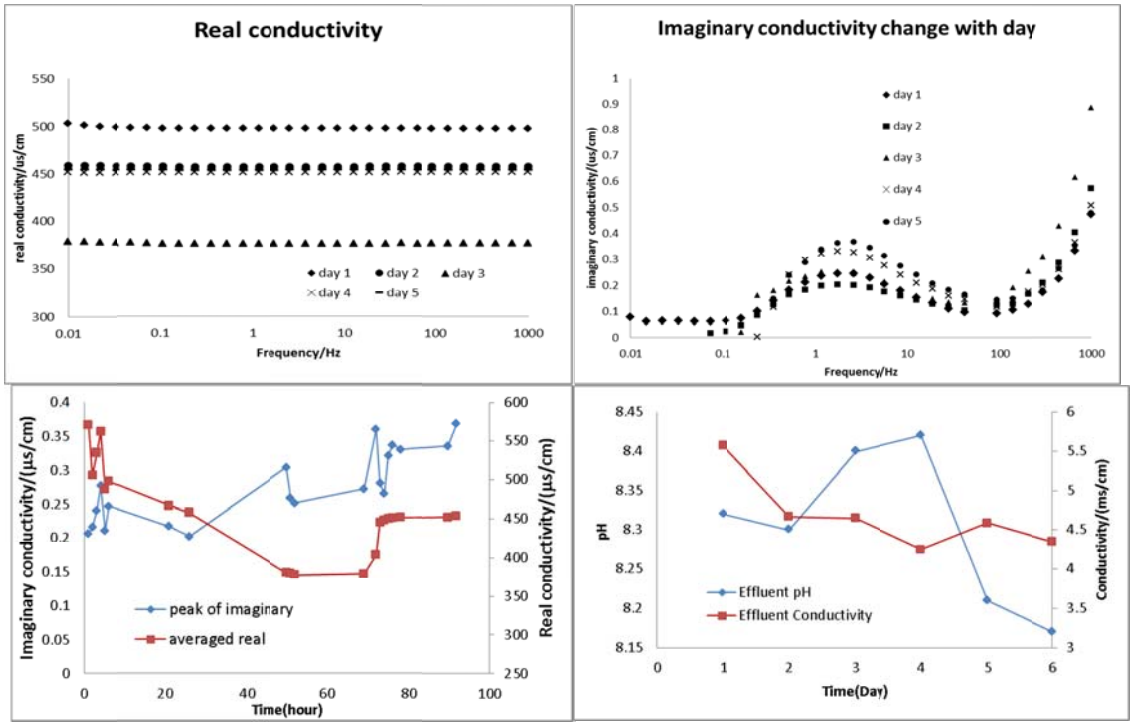

Figure 25: SIP results from the biologically mediated calcite precipitation experiment.

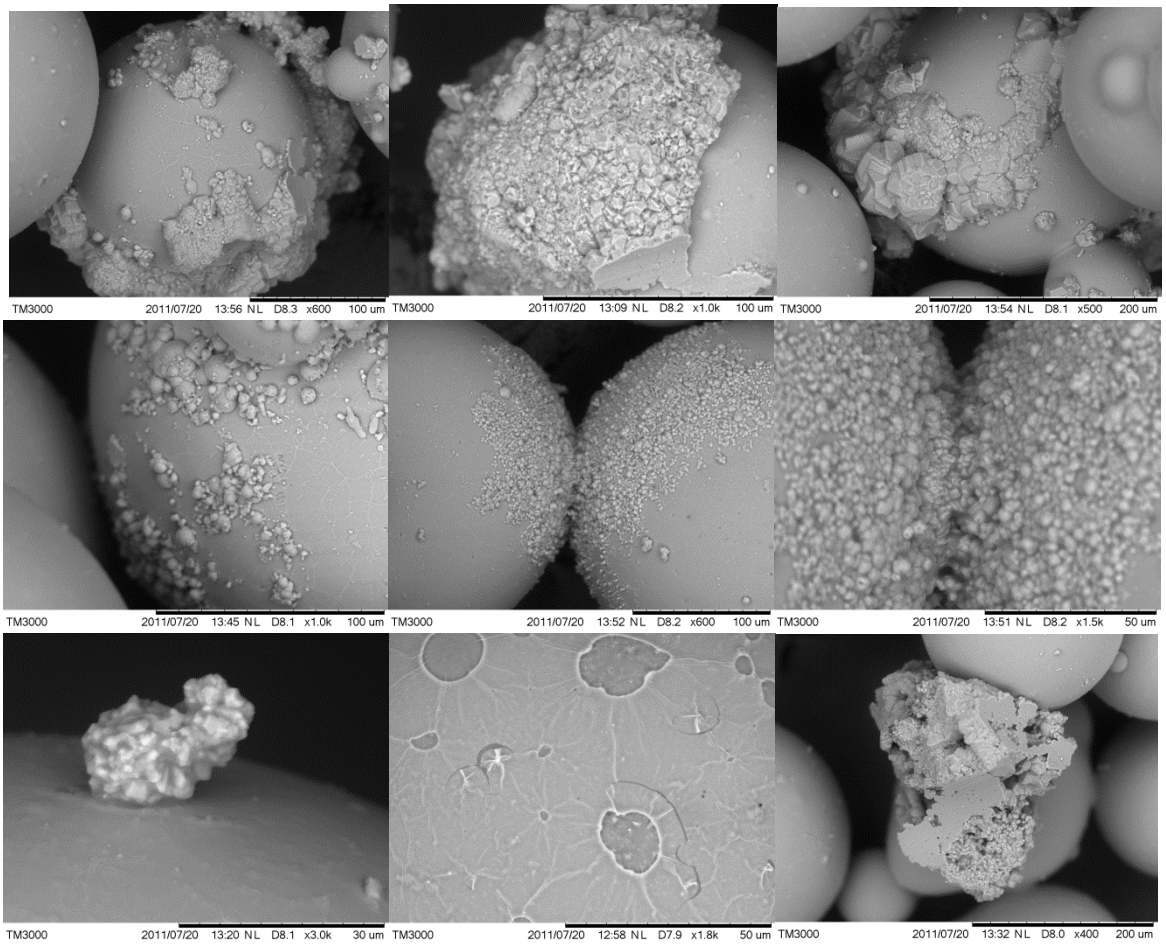

Figure 26: Examples calcium carbonate precipitates formed during the column flow experiment. Note the variety of morphologies formed, including cubic crystals, globular clusters, and sheets. Also featured are examples of precipitates at the contacts of grains and filling the interior pore volume (note flat areas on the precipitate cluster in the lower right and top center image).

2.2 Direct Measurement of Surface Properties by Atomic Force Microscopy (AFM)

One of the key goals in the project was to evaluate the use of atomic force microscopy (AFM) for understanding the electrical properties of surface at the grain scale. There are several different approaches to the problem that we explored in this project. The first approach used standard AFM measurements of surface roughness and charge density to provide indirect data on the surface electrical properties. In the initial part of the project the original project PI (Treavor Kendall) also initiated the modification of conductive force miscroscopy (CFM) methods for obtaining local frequency-domain measurements of complex conductivity at points on the grain surface. After Kendall left the project and it was transferred to Moysey and Dean, problems in the technique were found that impaired our ability to accurately perform these measurements under different experimental conditions. In response, we have developed a new technique for making time-domain measurements at the scale of individual grains that we feel has substantial promise for studying polarization processes at the grain scale. Example results from each of these efforts are discussed in more detail below.

2.2.1 Surface Roughness and Charge Density Mapping

Standard protocols for mapping topography and charge density with the AFM were followed to obtain data on these properties in parallel with the SIP experiments modifying the physical characteristics of the grains described above. The topography maps show that the etching, iron oxide and carbonate precipitates affected the topography of the beads. The surface charge density can be calculated from the data using a linearized Poission-Boltzmann model, allowing charge density to be mapped. Only surface charge that is fixed, however, can be measured; i.e., high electrical conductivities will allow charge to migrate in response to the fixed charge on the AFM tip thus impeding these measurements that are dependent on electrostatic attraction. These measurements are therefore relevant to SIP given that fixed surface charge is fundamentally important in attracting the ions that form the Stern and diffuse layers contributing to low frequency polarization. The charge density maps in Figure 27 indicate that the carbonate coated beads have the most measurable fixed negative charge relative to the other samples. This finding is consistent with the strong SIP responses that were observed when grain surfaces were treated with calcite.

2.2.2 Conductive Force Microscopy (CFM)

The original project plan proposed by Trevor Kendall (original project PI) was to modify traditional AFM methods to utilize an AC electric field, thereby evaluating point-scale complex conductivity measurements on grain surfaces. Kendall made progress on this effort by illustrating the impact of increasing relative humidity on the complex conductivity of a grain surface for untreated grains and grains pre-soaked in a saline solution (i.e., “salted” grains). Figures 29 illustrates how the time-domain response of the AFM varied as a function of relative humidity, producing increases in current amplitude and a decrease in phase; the trends in the estimated conductance and phase are plotted as a function of relative humidity in Figure 30. Figure 31 illustrates typical spectra obtained for a variety of grain treatments and values of relative humidity measured by Kendall. After Kendall left the project, the approach was applied at Clemson by co-PI Dean to measure properties of the treated grains used in the SIP experiments (Figure 32). Although the measurement appeared to have some early promise, several challenges were identified. First, after detailed investigation and discussion with the AFM manufacturer (Asylum Research), it was determined that it is not possible to make accurate frequency-domain phase measurements with the AFM due a lack of phase locking between the applied voltage and measured tip current. Additionally, concerns emerged that the conductive AFM measurements may not be sensitive to surface properties alone, particularly when the measurements are made in a fluid – a necessary condition for making meaningful comparisons to the SIP measurements.

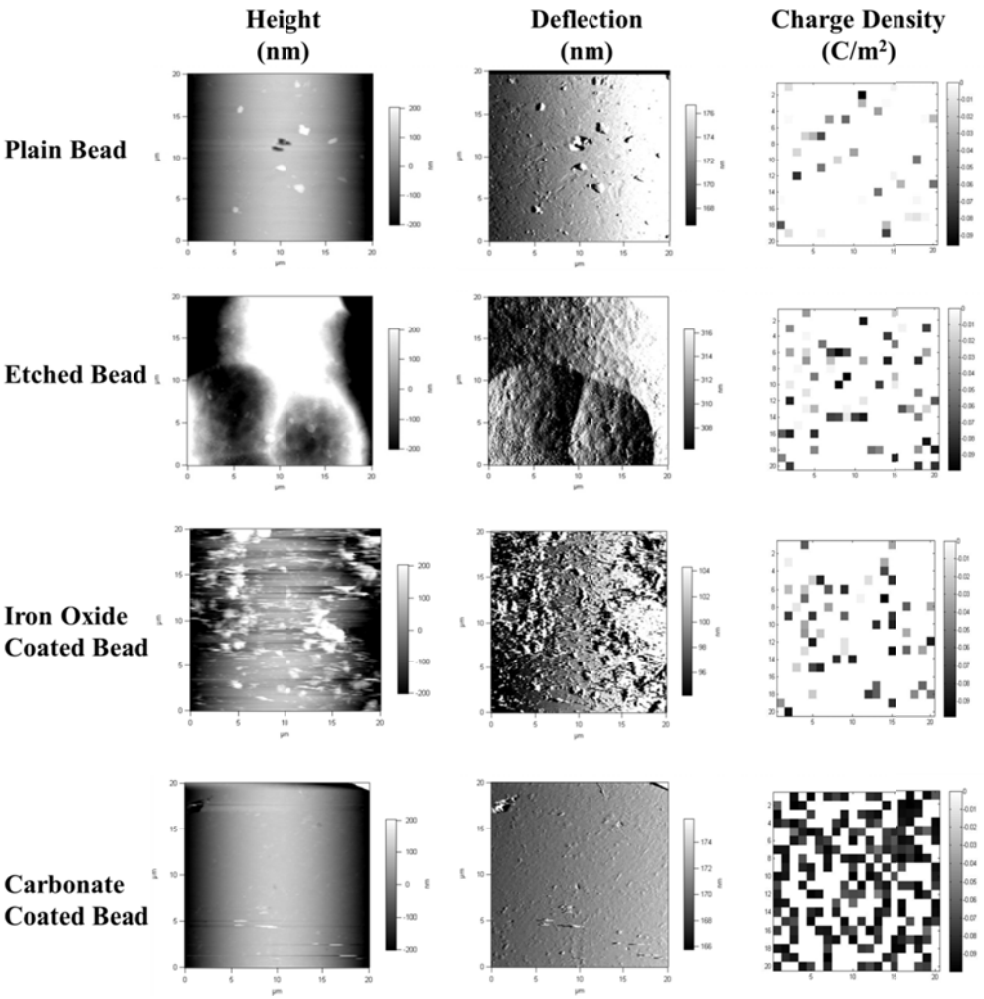

Figure 27: Height (left), Deflection (middle), and corresponding calculated surface charge density (right) of different bead surfaces as measured by AFM in 0.001M NaCl solution using a probe coated with a carboxyl terminated self-assembled monolayer. In solution, the carboxyl groups on the tip dissociate and the tip has a net negative surface charge ~0.02 C/m2. The area of each image is 20x20 μm.

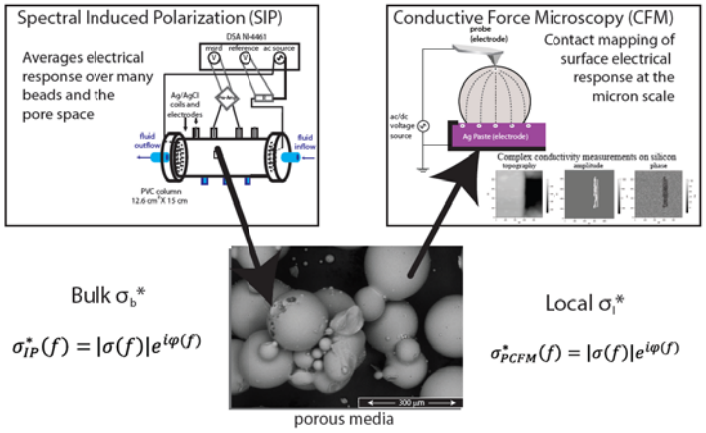

Figure 28: The original conceptual approach to integrating SIP and AFM in this project was to use conductivity force microscopy to measure grain surface properties. This is a contact measurement that utilizes an electric field applied between the charged tip and a plate electrode to measure variations in the conductive properties of materials.

Figure 29: Example time-domain data illustrating the applied voltage and current response using CFM. The approach was successfully applied to measure changes in conductivity associated with successively increasing the thickness of water on a grain surface by manipulating relative humidity.

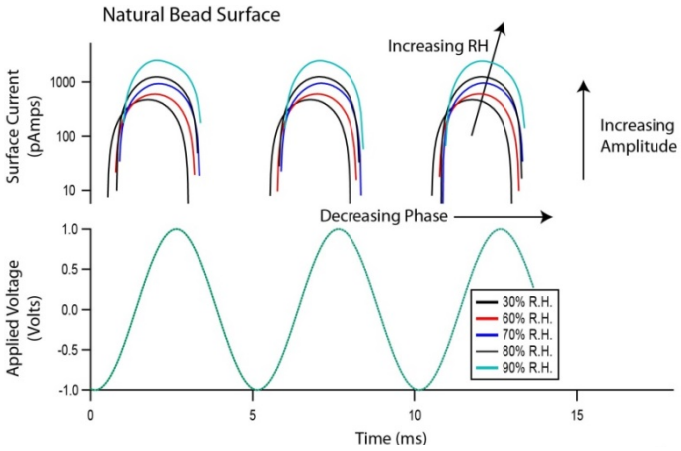

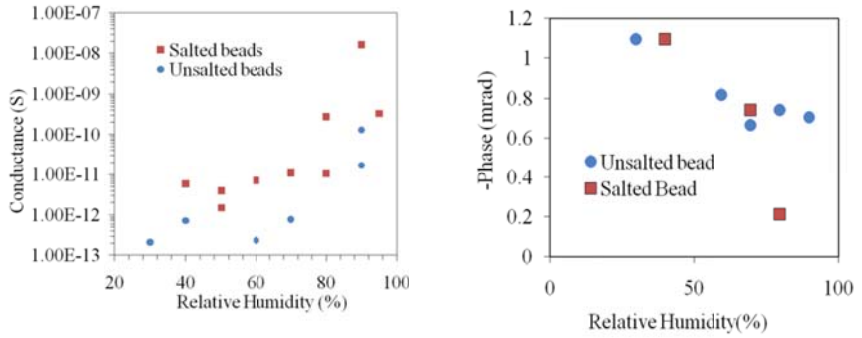

Figure 30: Trends in grain surface conductance (left) and phase (right) in response to increasing relative humidity.

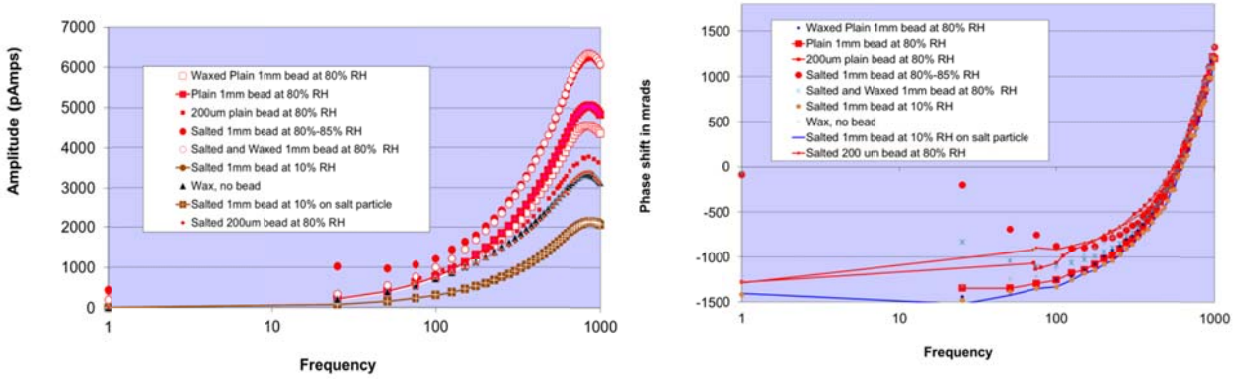

Figure 31: Amplitude and phase response measured for a variety of test scenarios and varying relative humidity.

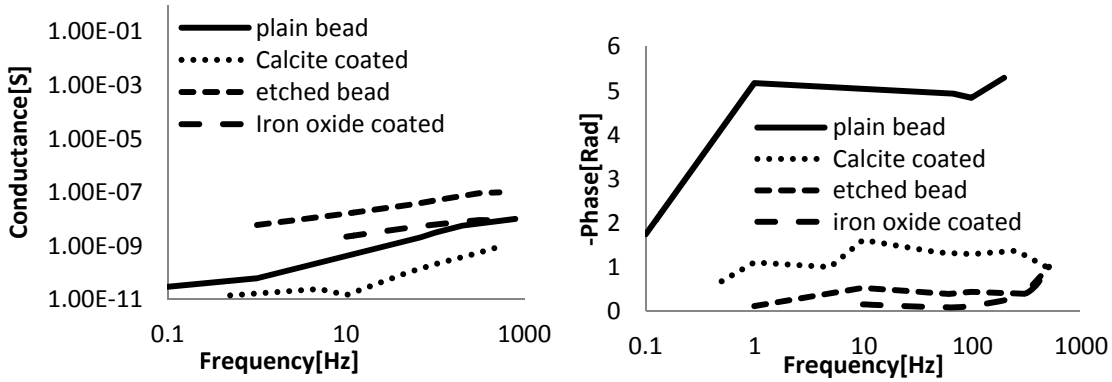

Figure 32: Comparison of conductance and phase measured for different glass bead treatments.

2.2.3 Time-Domain Polarization Measurements with AFM

Given the challenges faced with frequency domain polarization measurements, we adjusted our focus to evaluating methods to measure polarization effects with the AFM in the time domain. As a result, we have developed a novel AFM technique to measure charge polarization induced by an externally applied field. In this case, the sample (i.e., grain, bacterium, biofilm, etc.) is placed in a fluid-filled sample holder with embedded electrodes that allow for the application of a uniform electric field across the sample (Figure 33). A fixed charge is placed on the tip sorption. By placing the charged tip near one side of a polarized feature (e.g., grain), the force produced by the interaction between the polarized charge and a fixed test charge on the AFM tip will cause a defection of the tip that can be recorded at the nanometer scale by the AFM (Figure 34). By varying the applied external field, e.g., as square wave, it is possible to monitor tip deflections through time and relate these to the magnitude of grain polarization. The Fourier transform can then be used to relate these time domain measurements to the frequency domain responses obtained by SIP. The technique therefore allows for the direct measurement of charge accumulation resulting from polarization of the sample. Given that the tip can be scanned to different positions on the sample, it may also be possible to measure charge accumulations across the surface of a sample; though this has not yet been tested. Additionally, we expect that it will be possible to monitor biogeochemical influences on grain polarization through time, e.g., due to changes in fluid chemistry or mineral precipitation on the sample surface, because the sample holder can be modified to allow for the through flow of fluids.

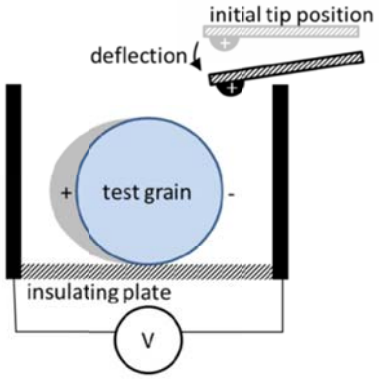

Figure 33: Schematic of setup for the AFM grain polarization measurement. The deflection of a charged AFM tip is used to evaluate the deflection associated with polarization of a grain in response to an externally applied electric field.

Our initial results evaluating this method have been promising, as we have been able to clearly distinguish between control and test samples. An example of the time-domain data is shown in Figure 34. One of the major problems we have encountered so far has been possible interference from glue used to attach the grains to the bottom of the sample holder. An inconsistent response for control measurements made directly on the glue has made it difficult to accurately interpret the influence of the glue on the grain measurements. The glue is necessary to prevent the grains from moving as the deflection measurements we have observed are on the order of tens to hundreds of nanometers. We have evaluated several different options to affix the grain to the sample holder, including varying adhesives and partially embedding the grains on the surface of epoxy disks. Though we have not yet found a clear solution to this problem, this appears to be the main challenge in the measurements and we will continue to attempt to identify various sample preparation methods beyond the scope of this project.

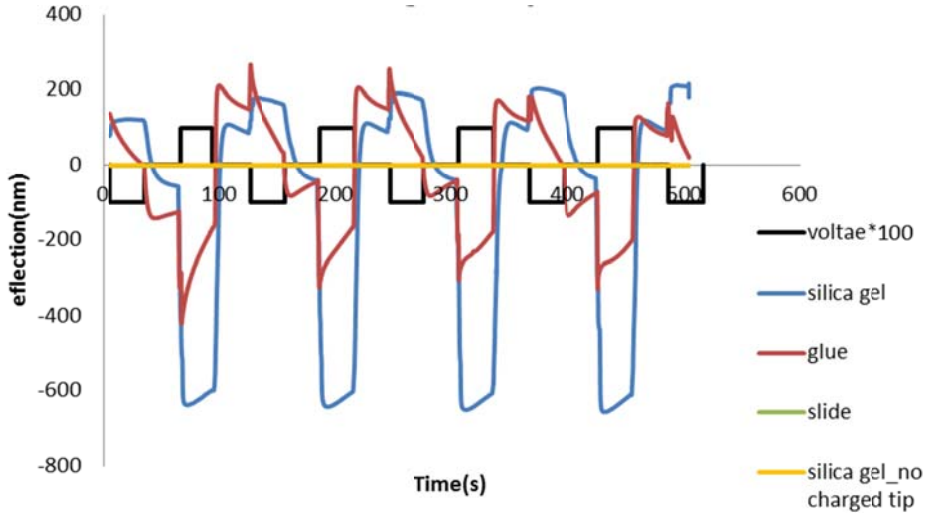

Figure 34: AFM tip deflection response observed in response to an applied voltage (black; actual value multiplied by 100 for scale) for silica gel (blue), background measurements on glue used to attach the silica gel to the sample holder (red). Control measurements on glass and when the AFM tip has no fixed charge show no response (green and yellow, respectively). Response shown is the average of 3 measurements.

3. Conclusions

The project was successful in exploring various mechanisms contributing the SIP response related to biogeochemical processes. We found an excellent correlation between complex conductivity and changes in pH and ion sorbed to the mineral surface. Both effects are related to effects within the Stern and diffuse layer and appear to be consistent with the triple layer model of the surface. Physical modifications of the surface illustrated that precipitates have a significant impact on SIP responses. Iron oxides, which appear to have a high conductivity but low fixed surface charge, caused a reduction in the imaginary conductivity of silica gel. In contrast, insulating calcite grains with a higher fixed surface charge provided a large and positive change to the complex conductivity. Traditional AFM measurements of surface charge density were found to be a useful tool for characterizing expected trends in the surface electrical properties of the samples. A new approach for measuring grain-scale polarization via deflection of a charged tip near a sample under an externally applied field also provided qualitative information of polarization responses, though further development of the method is required.

4. References Cited

Leroy, P., A. Revil, A. Kemna, P. Cosenza, and A. Ghorbani, 2008, Complex conductivity of water-saturated packs of glass beads, *Journal of Colloid and Interface Science*, **321**(1), 103-117.

Skold, M., A. Revil, and P. Vaudelet, 2011, The pH dependence of spectral induced polarization of silica sands: Experiment and modeling, *Geophysical Research Letters*, 30, L12304, doi:10.1029/2011GL047748.

5. Scholarly Products Resulting From this Work (* indicates student authors)

Hao, N., R. Chen, **S.M. Moysey**, D. Dean, D. Ntarlagiannis, K.Keating, 2011, Electrical response of modified grain surfaces using micron-scale atomic force microscope measurements and column-scale spectral induced polarization, Second International Workshop on Induced Polarization in Near-Surface Geophysis, Golden, Colorado, Oct.31-Nov.2 (poster).

Chen, R., N. Hao, M. Cupelli, **S.M.J. Moysey**, D. Dean, 2011, Analyzing microbial activity with the help of AFM by obtaining surface roughness and electrical properties of glass beads, Society for Biomaterials.

Hao*, N., J. Waterman*, T. Kendall, **S. Moysey**, D. Ntarlagiannis, 2010, Resolving biological-IP mechanisms using micron-scale surface conductivity measurements and column SIP data (poster), Goldschmidt Conference, Knoxville, June 15.

Posters at SBR Program Meetings:

*Hao, N., R. *Chen, **S.M.J. Moysey**, D. Dean, D. Ntarlagiannis, and K. Keating, 2012, Electrical responses of grain surfaces measured by spectral induced polarization and atomic force microscopy, DOE SBR PI Meeting, Washington, D.C., April (poster).

*Hao, N., R. *Chen, D. Dean, **S.M.J. Moysey**, D. Ntarlagiannis, and K. Keating, 2011, Electrical response of abiotically modified grain surfaces as observed with spectral induced polarization and atomic force microscope measurements, DOE SBR PI Meeting, Washington, D.C., April (poster).

Kendall, T., **S. Moysey**, D. Ntarlagiannis, J. Waterman*, and N. Hao*, 2010, Resolving biological-IP mechanisms using micron-scale surface conductivity measurements and column SIP data, DOE ERSP Annual Meeting, Washington D.C., March.